IOP Publishing Nanotechnology
Nanotechnology 27 (2016) 325702 (6pp) doi:10.1088/0957-4484/27/32/325702

Origin of blue photoluminescence from colloidal silicon nanocrystals fabricated by femtosecond laser ablation in solution

H L Hao[1], W S Wu[1], Y Zhang[1], L K Wu[2] and W Z Shen[2]

[1] College of Material Engineering, Shanghai University of Engineering Science, 333 Long Teng Road, Shanghai 201620, People's Republic of China
[2] Institute of Solar Energy, and Key Laboratory of Artificial Structures and Quantum Control (Ministry of Education), Department of Physics and Astronomy, Shanghai Jiao Tong University, 800 Dong Chuan Road, Shanghai 200240, People's Republic of China

E-mail: huilian.hao@sues.edu.cn and wzshen@sjtu.edu.cn

Received 24 February 2016, revised 30 May 2016
Accepted for publication 2 June 2016
Published 27 June 2016

Abstract

We present a detailed investigation into the origin of blue emission from colloidal silicon (Si) nanocrystals (NCs) fabricated by femtosecond laser ablation of Si powder in 1-hexene. High resolution transmission electron microscopy and Raman spectroscopy observations confirm that Si NCs with average size 2.7 nm are produced and well dispersed in 1-hexene. Fourier transform infrared spectrum and x-ray photoelectron spectra have been employed to reveal the passivation of Si NCs surfaces with organic molecules. On the basis of the structural characterization, UV–visible absorption, temperature-dependent photoluminescence (PL), time-resolved PL, and PL excitation spectra investigations, we deduce that room-temperature blue luminescence from colloidal Si NCs originates from the following two processes: (i) under illumination, excitons first form within colloidal Si NCs by direct transition at the X or Γ ($\Gamma_{25} \rightarrow \Gamma'_2$) point; (ii) and then some trapped excitons migrate to the surfaces of colloidal Si NCs and further recombine via the surface states associated with the Si–C or Si–C–H_2 bonds.

Keywords: colloidal silicon nanocrystals, femtosecond laser ablation, photoluminescence

(Some figures may appear in colour only in the online journal)

Over the previous decade, silicon (Si) nanocrystals (NCs) with visible luminescence have attracted extensive interest because of their high natural abundance and high compatibility to optoelectronic devices, which have great potential applications in light emitting diodes and next generation photovoltaic devices [1, 2]. Moreover, compared with luminescent but highly poisonous II-VI NCs (e.g., CdS, CdSe), the biocompatibility and environment-friendless of Si NCs make them more attractive in fluorescent labels and biological sensors [3, 4]. The previous focus was mainly on the light emission from Si NCs terminated with hydrogen. Experimental investigations suggest that Si NCs passivated with hydrogen are prone to agglomeration and oxidation, which can cause a serious shift and fading of photoemission, resulting in unstable and poor optical properties [5].

Colloidal Si NCs, the surfaces of which are capped with organic ligands through the formation of covalent Si–C bonds from organic molecules, have been the subject of intensive studies in recent years, because of their small size distribution, high luminescence quantum yields and dispersibility in solution. The organic molecules passivating the surface of Si NCs can prevent agglomeration of Si NCs by steric barriers or electrostatic repulsion, which has been proven to be very important in controlling and stabilizing the optical properties of Si NCs [6]. To date, several synthetic procedures have been developed for colloidal Si NCs. However, among these, some need two or more steps, resulting in a time consuming and complicated process; furthermore, these processes need poisonous agents and deoxygenated conditions, which leads to the production of toxic by-products [4, 7, 8].

Very recently, pulsed laser ablation in solution has attracted much attention in colloidal Si NC fabrication, which is a convenient and green method without any unnecessary by-products. The laser plasma plume formed during ablation and confined within the liquid media is an ideal environment to promote non-equilibrium processes, which can facilitate the formation of colloidal Si NCs [9]. Some works have demonstrated the viability of producing blue-emitting colloidal Si NCs via the laser ablation of bulk Si in water and organic solutions [10–13], and several luminescence mechanisms have been proposed, such as (i) quantum confinement effect (QCE) [14], (ii) direct band gap transition [15], (iii) QCE combined with surface states [16], and (iv) oxide-related radiative recombination of electron–hole pairs via surfaces of colloidal Si NCs [17]. Nevertheless, the microscopic origin of the blue luminescence from colloidal Si NCs has not been clarified yet, and there is not a consensual interpretation. To clarify the origin of the blue luminescence of colloidal Si NCs, the combined use of a tunable excitation laser source and time-resolved spectroscopy is very important to a thorough understanding of the excitation and emission pathway. This can reveal not only the transition and radiative recombination processes of electron–hole pairs but also the decay kinetics from the excited states, detailed analysis of which is indispensable to fully understand the mechanism of the blue luminescence and extend the applications of colloidal Si NCs.

In this work, colloidal Si NCs were synthesized by pulsed femtosecond laser ablation of single-crystal Si powder (>99.99%) with average size 100 nm in 1-hexene (>99%). The initial Si powder and 1-hexene were purchased from Aladdin reagent and Sigma Aldrich respectively. In preparing colloidal Si NCs, 15 mg Si powder was first dispersed in 5 ml 1-hexene in a glass vessel and ultrasonically rinsed for 30 min; then, pulsed Ti/sapphire laser (wavelength 800 nm, pulsed duration 100 fs and repetition of 1 kHz, focal length 10 cm, and laser fluence 0.15 mJ cm^{-2}) was used to irradiate the mixture of Si powder and 1-hexene for 2 h. During laser irradiation, the mixture was constantly stirred by a magnetic stirrer. After irradiation, the supernatant liquid was filtered by centrifugation at 11 000 rpm for 30 min with a membrane filter that had a pore size of 200 nm.

The formation and structure of colloidal Si NCs were confirmed by x-ray diffraction (XRD) and high resolution transmission electron microscopy (HRTEM, JEOL JEM-2100F). Raman scattering spectra were performed on a Jobin Yvon LabRAM HR 800 UV micro-Raman spectrometer using 514.5 nm line of Ar ion laser. Infrared absorption spectra (FTIR) were measured at Nicolet Nexus 870 Fourier transform infrared spectrometer within 400–4000 cm^{-1} range. The bonding configurations were analyzed by the x-ray photoelectron spectroscopy (XPS) spectra with a Shimadzu Kratos Axis Ultra DLD spectrometer using a monochromatic Al Kα x-ray source (1486.6 eV), and UV–visible (UV–vis) absorption spectra were measured by a Perkin-Elmer Lambda 20 spectrometer. Steady-state photoluminescence (PL) and PL excitation (PLE) spectra were recorded by Edinburgh Instruments FLS920 through normalizing the variation in Xe lamp output over the spectral range of interest. Time-resolved PL was measured by using a 405.0 nm diode laser with a pulse width of 60.0 ps as the excitation source. During the time-resolved luminescence measurements, the laser triggering, the wavelength scanning, the data acquisition and storage were controlled using a computer and custom software with Labview and Matlab.

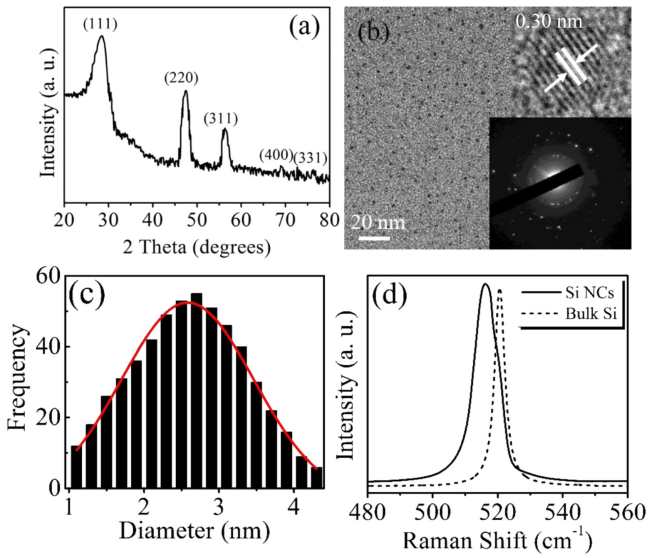

Figure 1. (a) XRD pattern of the colloidal Si NCs prepared in 1-hexane, (b) a typical HRTEM image of colloidal Si NCs, (c) the corresponding size distribution, and (d) room-temperature Raman spectra of colloidal Si NCs as in figure 1(b) and bulk Si. Upper inset: a HRTEM image of a Si NCs; Lower inset: the selected-area electron diffraction pattern of colloidal Si NCs.

Figure 1(a) presents the XRD pattern of the sample prepared in 1-hexene. The diffraction peaks centered at 28.5°, 47.1°, 56.2°, 69.1° and 76.4° are identified as silicon phase with diamond structure (JCPDF-27-1402), corresponding to Si (111), Si (220), Si (311), Si (400), and Si (331) planes respectively [18]. It should be noted that no other products can be detected. The average size of colloidal Si NCs can be estimated from the full width half maximum (FWHM) of XRD peaks using Scherrer equation [19]:

$$D = K\lambda/\beta \cos\theta$$

Here D is the mean size of colloidal Si NCs, K is a dimensionless shape factor with constant 0.89 for sphere, λ is x-ray wavelength of 0.151 48 nm, θ is Bragg diffraction angle of the peak, and β is FWHM of the peak.in radians. The calculated Si NCs size from the corresponding (111) diffraction peak is 2.64 nm.

A typical HRTEM image of Si NCs fabricated in 1-hexene is shown in figure 1(b), where Si nanoparticles appear as black dots and are found to be well dispersed. The average particle size is about 2.7 nm and thus to be nanocrystalline Si. The upper inset of figure 1(b) is a HRTEM image of a silicon nanocrystals with lattice fringes ~0.30 nm, corresponding to (111) of silicon [20–23]. To clearly understand the Si NCs structure, we have measured the selected-area electron diffraction pattern, displayed in the lower inset

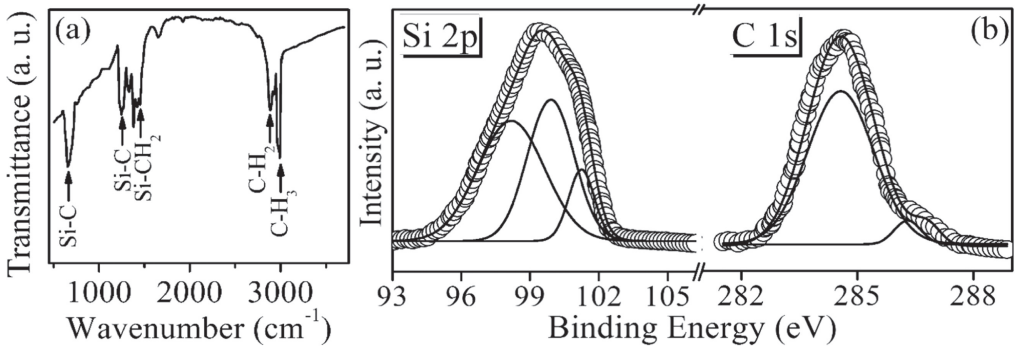

Figure 2. Room-temperature (a) infrared absorption spectrum and (b) the experimental (open circles) and calculated (solid curves) of Si 2p and C 1s XPS spectra for colloidal Si NCs prepared in 1-hexene.

of figure 1(b), which shows a ring pattern, suggesting that the Si NCs are crystalline. Different rings correspond to the different lattice planes of silicon, similar results have been reported in Si NCs embedded in SiO_2 matrix [24]. The statistics of the size distributions of Si NCs calculated from HRTEM measurements is displayed in figure 1(c), the mean diameter is 2.7 nm with a standard deviation of 0.5 nm, in good consistency with XRD results.

The structure and average size of Si NCs can be further confirmed by Raman measurements, as shown in figure 1(d). It can be clearly observed that the Raman peak position identified at 516 cm^{-1} of Si NCs shifts to lower wavenumber compared with that of bulk silicon crystalline (520 cm^{-1}), as well as a broadening of the full width at half maximum (FWHM) of Raman spectrum [25]. Both the redshift of Raman peak position and broadening of Raman spectrum, with respect to those of bulk silicon crystal, demonstrate the existence of phonon confinement effect. The dependence of the Raman peak position redshift ($\Delta\omega = -4$ cm^{-1}) on the Si NCs size (d, in nm) can be described through the phenomenological law [10]: $\Delta\omega = -19.856/d^{1.586}$. Here, the calculated Si NCs size is 2.74 nm, in good agreement with the size distribution 2.7 $\pm$ 0.5 nm as in figure 1(c).

Figure 2(a) shows the FTIR spectrum of the Si NCs as in figure 1(a), which can directly reveal the chemical bonds inside Si NCs. The absorption bands at 670, 1258, 1455, 2860, and 2960 cm^{-1} can be assigned to the modes of Si–C asymmetric vibration, Si–C asymmetric vibration, Si–CH_2 bending, symmetric C–H_2 stretching, and asymmetric C–H_3 stretching respectively [26, 27]. The formation of Si–C bonds indicates that the Si NCs surfaces have been passivated by carbon atoms.

Further insight into the bonding configurations of colloidal Si NCs can be achieved by XPS measurements. Figure 2(b) shows the experimental (open circles) and well fitted (solid curves) Si 2p (left) and C 1s (right) core-level binding energy spectra of colloidal Si NCs. Through Gaussian fitting, three dominant peaks at 98.3, 99.9, and 101.1 eV correspond to Si(0), Si(I), and Si(II) in Si 2p spectrum respectively. The Si(I) and Si(II) contributions are assigned to surface silicon atoms covalently attached to the more electronegative carbon atoms linking the Si NCs surface to pendant alkyl groups [28], further confirming that the Si NCs surfaces are well passivated by carbon atoms. For the C 1s XPS spectrum, the two dominant Gaussian peaks located at 284.7 and 286.2 eV correspond to C–H and Si–C bonds respectively [29]. This further indicates that the surfaces of Si NCs have been well passivated by carbon atoms, in good agreement with the FTIR results.

To investigate the passivation effect of colloidal Si NCs surfaces, the cover-degree of Si NCs surfaces by carbon atoms can be obtained as follows. The ratio of the whole area of the Si 2p peak to that of the Si–C bonds centered at 286.2 eV in C 1s XPS spectrum is 6.5. According to theoretical calculations, a pure Si NC with mean diameter 2.37 nm contains 278 Si atoms [30]. Consequently, there are 240 Si atoms with a mean diameter of 2.74 nm and 37 Si–C bonds on Si NCs surfaces for each Si NCs. So, the number of surface sites is assumed to be 86. As such, the mean surface coverage of the Si NCs with carbon is about 43%. The passivation mechanism is that, during laser ablation, Si NCs will have very high free energy and the surfaces of some Si atoms are unsaturated and active under extreme conditions, which can react with surrounding 1-hexene and a cyclic compound will be formed. This can be well expressed by the chemical reaction in ablation process [26]:

Here, R represents $(CH_2)_3CH_3$. Therefore, the Si–C bonds are expected to be formed at the surfaces of Si NCs.

Figure 3 displays the UV–vis absorption spectrum of colloidal Si NCs. A long absorption tail in wavelength >600 nm range and the dominant absorption peak at 270 nm (4.5 eV) can be clearly observed. The long absorption tail reflects the indirect band gap electronic structure of crystalline Si. The absorption edge shifts toward shorter wavelength (higher energy) compared with that of bulk Si crystal (~1125 nm), indicating the existence of QCE [11, 27]. The QCE will not only influence the indirect band gap but also the direct transition energies. Due to QCE, the direct transition energy at X or Γ ($\Gamma_{25} \rightarrow \Gamma'_2$) point within Si NCs presents 0.3 eV blueshift compared with that of bulk Si crystal (4.2 eV), leading to the emergence of the absorption peak at 270 nm (4.5 eV) [31].

Figure 4(a) presents the room-temperature PL spectra of colloidal Si NCs excited under different wavelengths. It can be observed that the emission peaks centered at 412 nm (~3.0 eV) are independent of excitation wavelength (λ_{exc}) in

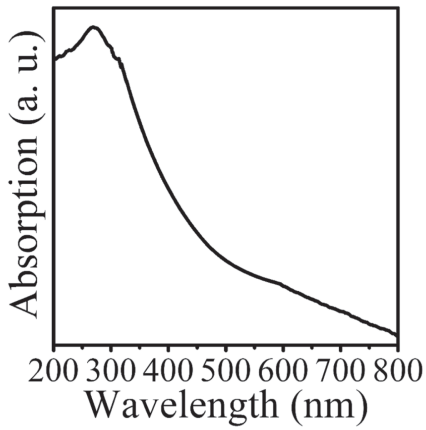

Figure 3. UV–vis absorption spectrum of colloidal Si NCs prepared in 1-hexene.

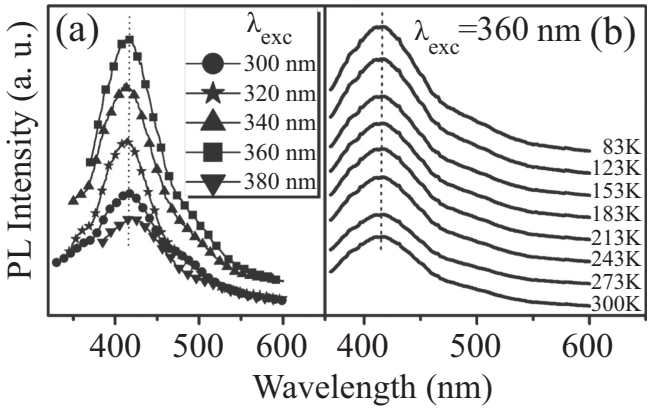

Figure 4. (a) Room-temperature PL spectra at the indicated excitation wavelength and (b) temperature-dependent PL spectra of colloidal Si NCs with excitation wavelength 360 nm.

the 300–380 nm range. The FWHM of the PL spectra decreases from 107.4 nm (~0.63 eV) in the Si NCs excited with $\lambda_{exc} = 300$ nm to 95.6 nm (~0.58 eV) in the one with $\lambda_{exc} = 380$ nm. With increasing λ_{exc}, a significant improvement of the emission intensity can be observed, and the maximum luminescence intensity is obtained from colloidal Si NCs excited under $\lambda_{exc} = 360$ nm. With the further increase of λ_{exc} to 380 nm, the luminescence intensity drastically decreases.

Due to the combination of indirect and direct band gap transitions, the luminescence mechanism of colloidal Si NCs is complicated. To investigate the PL mechanism of colloidal Si NCs, we first performed temperature-dependent PL measurements. Figure 4(b) displays the typical results for colloidal Si NCs excited under $\lambda_{exc} = 360$ nm, where both emission peak position and FWHM are independent of temperature throughout the measured ranges. Moreover, the room-temperature PL peak energy is independent of excitation wavelength [see figure 4(a)]. Both these observations suggest that the PL mechanism is not determined by QCE [32]. In addition, it should be noted that no luminescence can be observed from 1-hexene alone irradiated by laser. As a result, we can assume that the blue PL should originate from colloidal Si NCs rather than the solution.

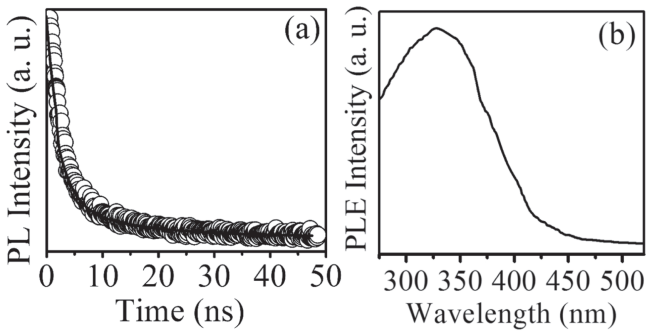

Figure 5. (a) Time-resolved PL spectra and (b) PLE spectra monitored at 3.0 eV for colloidal Si NCs.

In order to clarify the light emission mechanism of colloidal Si NCs, we have further carried out time-resolved PL and PLE measurements. Figure 5(a) shows the experimental (open circles) and calculated (solid curve) decay results for colloidal Si NCs fabricated in 1-hexene. The decay process can be accurately fitted by a double exponential function: $I(t) = A_1 e^{-t/\tau_1} + A_2 e^{-t/\tau_2}$, where $I(t)$ is the PL intensity as a function of time t; A_1, A_2, τ_1 and τ_2 are the fitting constants. The colloidal Si NCs exhibit a fast decay component with lifetime 0.8 ns and a slow one with lifetime 5.0 ns. First-principles calculations of optical properties of Si NCs have revealed that the nanosecond decay time can be attributed to localized exciton transitions at the surfaces of the Si NCs, where the fast and slow decay components correlate, respectively, to the nonradiative excitons' trapping time at the X or Γ ($\Gamma_{25} \rightarrow \Gamma'_2$) point and recombination (both radiative and nonradiative) of the trapped excitons [33]. The average decay times $\bar{\tau}$ can be calculated through formula: $\bar{\tau} = (A_1\tau_1^2 + A_2\tau_2^2)/(A_1\tau_1 + A_2\tau_2)$, and $\bar{\tau}$ is obtained to be 4.2 ns, the fitted constants $A_1 = 59.4\%$ and $A_2 = 40.6\%$. The PL lifetime in the order of nanoseconds indicates that colloidal Si NCs solution has a large radiative decay rate similar to those of direct band gap semiconductors, consistent with the results shown in figure 3. The fast radiative recombination rate is very important for biomedical applications.

We now focus on the radiative recombination process of the localized state excitons. Figure 5(b) displays the PLE spectrum of colloidal Si NCs with the detection energy of 3.0 eV [see figure 4(a)]. The PLE spectrum exhibits the absorption peak at 326 nm (3.8 eV) and a long tail in the visible range, in good agreement with the UV–vis absorption results. Compared with the PL peak energy, the PLE peak has a large Stokes shift of 0.8 eV for colloidal Si NCs. The configuration coordinate mode is usually used to describe the large Stokes shift and broadening of the luminescence spectra of Si NCs [31]. In this model, the coupling between the electronic state and the lattice occurs through transverse acoustic phonons with a single frequency Ω, and the Stokes shift has the form $E_S = A^2/(M\Omega^2)$, with A a constant and M the mass of the coupling phonon. The coupling phonon energy can be expressed as $\hbar\Omega = W^2|_{T\rightarrow 0}/(4 \ln 2)E_S$, where W is the FWHM of the PL spectrum, and it keeps unchanged

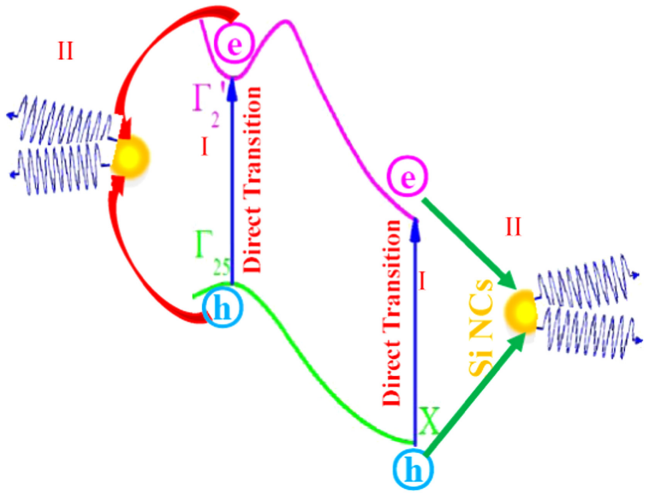

Figure 6. Schematic diagram of the blue emission from colloidal Si NCs.

over the investigated temperature range in figure 4(b). The phonon energy $\hbar\Omega$ is found to decrease continuously from 107.4 nm (0.63 eV) in the sample excited with $\lambda_{exc} = 300$ nm to 95.6 nm (0.58 eV) in the one with $\lambda_{exc} = 380$ nm. Moreover, the energies of 0.180 eV ($\sim$1455 cm^{-1}) and 0.56 eV ($\sim$1258 cm^{-1}) correspond well to Si–C and Si–C–H_2 vibration modes respectively. This indicates that the PL mechanism is related to the electron–hole pairs recombination associated with Si–C or Si–C–H_2 vibration phonons. On the basis of the above analyses, we conclude that the room-temperature blue luminescence of colloidal Si NCs prepared in 1-hexene originates from the following two processes, as schematically illustrated in figure 6: (i) When quantum-confined colloidal Si NCs are under excitation light illumination, excitons first form through the direct transitions at *X* or Γ ($\Gamma_{25} \rightarrow \Gamma'_2$) point (Process I); (ii) then some trapped excitons migrate to the surface states at the surfaces of colloidal Si NCs and further recombine via the surface states related to the Si–C or Si–C–H_2 bonds (Process (II).

After the detailed investigation of PL properties for colloidal Si NCs, we can explain the variations of FWHM and intensity of room-temperature luminescence. With the increase of λ_{exc}, the carriers in smaller Si NCs cannot be excited, thus leading to the decrease of FWHM [9]. At $\lambda_{exc} \leqslant$ 360 nm range, the significant improvement of PL intensity with the increase of the excitation wavelength can be explained as follows. With increase of the excitation wavelength from 300 to 360 nm, the quantum-confined Si NCs with the most probable sizes can always be excited and the emission intensity increases. With further increase of excitation wavelength, the smallest excitable size of Si NCs increases and the number of luminescent Si NCs decreases sharply, which sequentially quenches PL. Based on the these analyses, it is reasonable to assume that the 360 nm excitation corresponds to the resonant excitation condition of the most probably sized colloidal Si NCs, therefore, the maximum emission intensity can be obtained under $\lambda_{exc} = 360$ nm.

In summary, we have fabricated the blue-emitting colloidal Si NCs by femtosecond laser ablation in 1-hexene under ambient conditions, and investigated its structures and the origin of room-temperature blue emission in detail. The average size of colloidal Si NCs was about 2.7 nm via HRTEM and Raman measurements. FTIR and XPS spectra demonstrated that the surfaces of Si NCs were well passivated with organic molecules. Based on UV–vis absorption, temperature-dependent PL, time-resolved PL and PLE spectra, we conclude that the luminescence of colloidal Si NCs originates from the following two processes: (i) firstly, under illumination, excitons form within quantum sized colloidal Si NCs by direct transition at the *X* or Γ ($\Gamma_{25} \rightarrow \Gamma'_2$) point; (ii) secondly, some trapped excitons transfer to the surfaces of colloidal Si NCs and further recombine via the surface states associated with the Si–C or Si–C–H_2 bonds. Colloidal Si NCs synthesized by femtosecond laser ablation in 1-hexene with good surface passivation and stable optical properties will meet the expectation of optoelectronic devices and bioimaging.

Acknowledgments

This work was supported by the Natural Science Foundation of China under contracts 11504229 and 61234005, Shanghai 'YangFan' Project (No. 14YF1409500), the Research Fund for the Doctor Program of Shanghai University of Engineering Science under contract 201308 and Shanghai Youth College Teachers Training Program of ZZGJD13023.

References

[1] Umezu I, Minami H, Senoo H and Sugimura A 2007 *J. Phys.: Conf. Ser.* **59** 392–5
[2] Cheng K Y, Anthony R, Kortshagen U R and Holmes R J 2010 *Nano Lett.* **10** 1154
[3] Mastronardi M L, Maier-Flaig F, Faulkner D, Henderson E J, Kübel C, Lemmer U and Ozin G A 2012 *Nano Lett.* **12** 337
[4] Hessel C M, Reid D, Panthani M G, Rasch M R, Goodfellow B W, Wei J W, Fujii H, Akhavan V and Korgel B A 2012 *Chem. Mater.* **24** 393
[5] Botas A M P, Ferreira R A S, Pereira R N, Anthony R J, Moura T, Rowe D J and Kortshagen U 2014 *J. Phys. Chem.* C **118** 10375
[6] Sugimoto H, Fujii M, Imakita K, Hayashi S and Akamatsu K 2013 *J. Phys. Chem.* C **117** 6807
[7] Hessel C M, Rasch M R, Hueso J L, Goodfellow B W, Akhavan V A, Puvanakrishnan P, Tunnel J W and Korgel B A 2010 *Small* **6** 2026
[8] Portolés M J L, Nieto F R, Soria D B, Amalvy J I, Peurzzo P J, Mártire D O, Kotler M, Holub O and Gonzalez M C 2009 *J. Phys. Chem.* C **113** 13694
[9] Lu W B, Wu L P, Yu W, Wang X Z, Li X W and Fu G S 2012 *Micro Nano Lett.* **7** 1125
[10] Vaccaro L, Sciortino L, Messina F, Buscarino G, Agnello S and Cannas M 2014 *Appl. Surf. Sci.* **302** 62
[11] Yang S K, Cai W P, Zhang H W, Xu X X and Zeng H B 2009 *J. Phys. Chem.* C **113** 19091
[12] Intartaglia R, Barchanski A, Bagga K, Genovese A, Das G, Wagener P, Fabrizio E D, Diaspro A, Brandi F and Barcikowski S 2012 *Nanoscale* **4** 1271

[13] Švrček V, Sasaki T, Shimizu Y and Koshizaki N 2006 *Appl. Phys. Lett.* **89** 213113
[14] Švrček V, Sasaki T, Katoh R, Shimizu Y and Koshizaki N 2009 *Appl. Phys.* B **94** 133
[15] Zhou Z Y, Brus L and Friesner R 2003 *Nano Lett.* **3** 163
[16] Bagabas A A, Gondal M A, Dastageer M A, Al-Muhanna A A, Alanazi T H and Ababtain M A 2009 *Nanotechnology* **20** 355703
[17] Pi X D, Liptak R W, Nowak J D, Wells N P, Carter C B, Campbell S A and Kortshagen U R 2008 *Nanotechnology* **19** 245603
[18] Yang S K, Cai W P, Zeng H B and Li Z G 2008 *J. Appl. Phys.* **104** 023516
[19] Yu Y X, Rowland C E, Schaller R D and Korgel B A 2015 *Langmuir* **31** 6886
[20] Inada M, Nakagawa H, Umezu I and Sugimura A 2002 *Appl. Surf. Sci.* **197-198** 666
[21] Intartaglia R, Bagga K, Scotto M, Diaspro A and Brandi F 2012 *Opt. Mater. Express* **2** 510
[22] Intartaglia R, Bagga K, Brandi F, Das G, Genovese A, Fabrizio E D and Diaspro A 2011 *J. Phys. Chem.* C **115** 5102
[23] Alkis S, Okyay A K and Ortac B 2012 *J. Phys. Chem.* C **116** 3432
[24] Chaturvedi A, Joshi M P, Rani E, Ingale A, Srivastava A K and Kukreja L M 2014 *J. Lumin.* **154** 178
[25] Kuzmin P G, Shafeev G A, Bukin V V, Garnov S V, Farcau C, Carles R, Fontrose B W, Guieu V and Viau G 2010 *J. Phys. Chem.* C **114** 15266
[26] Tan D Z, Ma Z J, Xu B B, Dai Y, Ma G H, He M, Jin Z M and Qiu J R 2011 *Phys. Chem. Chem. Phys.* **13** 20255
[27] Nakamura T, Yuan Z and Adachi S 2014 *Nanotechnology* **25** 275602
[28] Dasog M, Reyes G B D L, Titova L V, Hegmann F A and Veinot J G C 2014 *ACS Nano* **8** 9636
[29] Wang Q, Ni H J, Pietzsch A, Hennies F, Bao Y P and Chao Y M 2011 *J. Nanopart. Res.* **13** 405
[30] Vasic M R, Spruijt E, Lagen B V, Cola L D and Zuilhof H 2008 *Small* **4** 1835
[31] Yang S K, Li W Z, Cao B Q, Zeng H B and Cai W P 2011 *J. Phys. Chem.* C **115** 21056
[32] Hao H L and Shen W Z 2008 *Nanotechnology* **19** 455704
[33] Negro L D, Yi J H, Michel J, Kimerling L C, Chang T W F, Sukhovatkin V and Sargent E H 2006 *Appl. Phys. Lett.* **88** 233109